Modeling of carbon monoxide two-photon LIF spectra at high temperature and pressure

Olivier Carrivain, Mikael Orain, Nelly Dorval, Céline Morin, G. Legros

Modelling of carbon monoxide two-photon LIF spectra at high temperature and pressure

O. CARRIVAIN[1], M. ORAIN[2*], N. DORVAL[1], C. MORIN[3], G. LEGROS[4]

[1]*ONERA-DPHY, ONERA, Université Paris-Saclay F-91123 Palaiseau, France*
[2]*ONERA-DMPE, ONERA, Université de Toulouse F-31055 Toulouse, France*
[3]*Univ. Polytechnique Hauts-de-France, CNRS, UMR 8201 – LAMIH, 59313 Valenciennes, France*
[4]*Sorbonne Universités, UPMC Univ Paris 06, CNRS UMR 7190, Institut Jean Le Rond d'Alembert, 75005 Paris, France*

Full-Length Article

STATEMENT

The content of this manuscript submitted to "Applied Spectroscopy" is unpublished material that is not being submitted for publication elsewhere.

Shortened Running Title

CO fluorescence modelling

[*] Corresponding author: Dr Mikael Orain
ONERA – The French Aerospace Lab
Tel: +33 5 61 56 63 48
Fax: +33 5 61 56 63 87
E-mail address: mikael.orain@onera.fr

ABSTRACT

In this study, we have developed a quantitative model of two-photon excitation and fluorescence spectra of carbon monoxide based on up-to-date spectroscopic constants collected during an extensive literature survey. This semi-classical model takes into account Hönl-London factors, quenching effects (collisional broadening and shift), ionisation and stark effect (broadening and shift), whereas predissociation is neglected. It has been specifically developed to first reproduce with a high confidence level the behaviour of our experimental spectra obtained from laser-induced fluorescence measurements, and then to allow us to extrapolate the fluorescence signal amplitude in other conditions than those used in these experiments. Synthetic two-photon excitation and fluorescence spectra of CO were calculated to predict the fluorescence signal at high pressures and temperatures, which are representative of gas turbine operating conditions. Comparison between experimental and calculated spectra is presented. Influence of temperature on both excitation and fluorescence spectra shapes and amplitudes is well reproduced by the simulated ones. It is then possible to estimate flame temperature from the comparison between experimental and calculated shapes of numerical excitation spectra. Influence of pressure on both excitation and fluorescence spectra was also investigated. Results show that for temperature below 600 K and pressure above 0.1 MPa, the usual Voigt profile is not suitable to reproduce the shape of the excitation spectrum. We found that the Lindholm profile is well suited to reproduce the pressure-dependence of the spectrum in the range 0.1 to 0.5 MPa at 300 K, and 0.1 to 0.7 MPa at 860 K. Beyond 0.7 MPa, in this temperature range, it is shown that the Lindholm profile does no longer match the spectral profiles, in particularly the red wing. Further analyses taking into account the line mixing phenomenon at higher pressure are thus discussed.

Keywords: LIF, carbon monoxide, spectroscopy, modelling, combustion

I. Introduction

Monitoring pollutant emissions from aircraft engines is crucial for gas turbine manufacturers. Indeed, regulations are becoming more and more stringent and, therefore require drastic reduction of emissions in the coming decade. Among pollutants released by combustion process, carbon monoxide (CO) is an extremely toxic combustion product widely generated in the fuel-rich low-temperature regions of the engines. Hence, a high level of CO is a good indicator of an incomplete combustion. It is therefore interesting to probe CO directly inside the combustor to better understand CO formation mechanisms and locate production areas. Laser diagnostics and more specifically Laser-Induced Fluorescence (LIF) are a suitable tool to obtain such information.

While a large amount of studies have experimentally [1-5] investigated carbon monoxide fluorescence, there are only a few attempts of CO fluorescence modelling reported in the literature [1-3, 6]. The simulation code developed by Seitzman et al. [1] for CO-LIF spectra in flames at atmospheric pressure (for B-X /B-A excitation/detection scheme) may not be adapted to high-pressure flame conditions, because collisional broadening and shift were approximately calculated, due to the lack of validation data in 1987. Furthermore, this code is limited to a high-laser-intensity regime for which CO ionisation is dominant with respect to the quenching regime. Similarly, the code from Linow et al. [2] allows to reproduce both C-X/C-A and B-X/B-A spectra only for specific flame conditions (i.e. 1900 K, 0.1 MPa). Di Rosa et al. [6] have developed a code that was dedicated to the determination of collisional broadening and shift coefficients for temperatures up to 1013 K and pressures up to 0.05 MPa. More recently, Rosell et al. [3] have developed a code that simulates only dispersed fluorescence spectra (one-photon) for $C^1\Sigma^+$-$A^1\Pi$, $B^1\Sigma^+$-$A^1\Pi$ and $b^3\Sigma^+$-$a^3\Pi$ transitions and signal variation with pressure (up to 0.5 MPa). Nonetheless, these authors do not report information on pressure influence on the excitation spectrum, contrary to the studies of Voigt et al. [7, 8], where simulated and experimental excitation spectra are compared at 1870 K and 0.5 MPa. However, among all these studies, none of them showed a code validation over a wide range of temperature and pressure. Additionally, no CO-LIF simulation code is available, neither for sale nor freely distributed like LIFSIM [9] and LIFBASE [10], in the spectroscopy community. Therefore, it is justified to develop a

simulation code of two-photon CO-LIF spectra that works for a large field of conditions and as robust as possible (taking into account three electronic transitions, large temperature and pressure ranges and different gas mixture compositions). The aim of the paper is to describe the modelling procedure which was developed to simulate CO-LIF spectra (two-photon excitation and one-photon dispersed fluorescence spectra) and for a large set of thermodynamic conditions. A first validation step of the spectra modelling is successfully achieved by comparison with our previous experimental results [4]. It is noted that all the models developed in the references [1-3, 6-8] and this paper are valid for pulsed lasers in the nanosecond regime. However, there is a recent interest for two-photon CO-LIF experiments and modelling with picosecond and femtosecond pulses [11-14]. For example, Li et al. [13] highlight the possible advantages of such short excitation pulses: a broadband excitation, a stronger fluorescence signal compared to that in the ns regime, simultaneous measurements of CO concentration and flame temperature by using the temperature dependence of the hot vibrational band (B(1)-X(1)) and rotational lines observed in fs-fluorescence spectra. Additionally, Kuchkina et al. [11] have recently developed a two-photon fluorescence signal model for ps and fs regimes, which can be used together with CO experiments in order to retrieve quantitative data. Nonetheless, although very interesting, this modelling approach is out of the scope of the current article which is dedicated to the modelling of CO-LIF spectra in the ns regime. The remaining paper is divided into three sections. Spectra modelling principle is firstly detailed for the three excitation/fluorescence schemes (A-X/A-X, B-X/B-A and C-X/C-A). To that end, an extensive literature survey has been realised in order to collect all spectroscopic data (spectroscopic constants, two-photon absorption cross-sections, collisional data, ionisation cross-sections...). Secondly, the influence of temperature on CO-LIF spectra is investigated and comparison between experiments and simulations are presented, for different temperatures at 0.1 MPa. In addition, temperature measurement in a methane/air flame is presented. Thirdly, pressure effects on simulated spectra are presented and compared to experimental data. The paper concludes with a summary of the results and future perspectives.

II. Spectra modelling principle

II.1. Theory

In the literature, three excitation/fluorescence strategies are generally considered for CO-LIF measurements in reactive flows (see. Fig.1):

- Carbon monoxide is two-photon pumped at 230.1 nm from the ground state ($X^1\Sigma^+$ (v''=0, J'')) to the excited state ($B^1\Sigma^+$ (v'=0, J')) which deactivates towards the lower-lying states ($A^1\Pi$(v=0-5, J) and $X^1\Sigma^+$), with fluorescence emission in the range 440 - 700 nm. Additionally, collisions can lead to non-radiative deactivation of the $B^1\Sigma^+$ state to the $b^3\Sigma^+$ triplet state, which emits fluorescence in the range 280 - 400 nm through the $b^3\Sigma^+$-$a^3\Pi_u$ transition. The B-X/B-A scheme is found to be the most used to probe CO in flames [4].

- Two-photon excitation in the fourth positive system ($A^1\Pi$ (v'=4,5)←←$X^1\Sigma^+$(v''=0)) in the range 278 - 284 nm and fluorescence detection through A-X(4,11-15) and A-X(5,11-15) vibrational bands was a strategy applied by Mosburger and Sick [5] for the simultaneous detection of CO and OH in a Bunsen burner flame. However, this approach requires the detection of fluorescence signal at short wavelengths (between 200 and 240 nm).

- Two photon excitation at 217.5 nm of the Hopfield band ($C^1\Sigma^+$(v'=0)←←$X^1\Sigma^+$(v''=0)) with detection through the Herzberg band ($C^1\Sigma^+$(v'=0)→ $A^1\Pi$ (v''=0)) in the range 400 - 600 nm have been demonstrated by Linow et al. [2].

Advantages and drawbacks of each approach have already been discussed in details in our previous paper [4]. The comparison between these three excitation/fluorescence strategies led us to choose the first scheme (B-X/B-A) for our experimental investigations. Nonetheless, the CO-LIF spectra modelling has been performed for these three schemes, and in the case of A-X and C-X systems, the calculated spectra were validated by comparison with published spectra obtained by other authors [15]. In the current paper, the modelling procedure is described for the B-X/B-A spectra by using the most reliable spectroscopic and collisional parameters collected from an extensive literature survey [15].

As mentioned by Seitzman et al. [1], fluorescence signal from a two-photon excitation, assuming linear polarization and laser intensity below the saturation level, can be expressed as:

$$S_{LIF} = \eta \frac{\Omega}{4\pi} N_{CO} \tilde{\sigma}^{(2)} \left(\frac{I_L}{h\upsilon_L} \right)^2 \Phi(T,P) \quad (1)$$

where η is the optical efficiency of the detection system, Ω the solid angle (Sr), N_{CO} the total number density of CO (cm^{-3}), $\tilde{\sigma}^{(2)}$ the two-photon absorption coefficient ($cm^4.s$), I_L the laser intensity ($W.cm^{-2}$), h the Planck constant (6.62×10^{-34} J.s), ν_L the laser frequency (Hz) and Φ(T,P) the fluorescence quantum yield function of the temperature T (K) and the pressure P (MPa). The two-photon absorption coefficient is given by:

$$\tilde{\sigma}^{(2)} = \sigma_0^{(2)} G^{(2)} f_{J''} \frac{S^{(2)}_{J'J''}}{2J''+1} \Gamma \quad (2)$$

where J', J'' are the quantum numbers for total rotational angular momentum in the upper and lower states, respectively, $\sigma_0^{(2)}$ the spectrally integrated two-photon absorption cross-section (cm^4), $G^{(2)}$ the second-order intensity correlation factor of the photon statistics of the excitation pulse which is set to 2 for the case of a multimode laser, $f_{J''}$ the fractional population in the rotational state $X^1\Sigma^+(v''=0, J'')$, $S_{J'J''}^{(2)}$ the two-photon Hönl-London factor, and Γ (cm^{-1}) the two-photon overlap integral given by:

$$\Gamma = \int_{-\infty}^{+\infty} \Phi_{J'J''}(\xi - \sigma_{J'J''}) g(\xi - 2\sigma_L) d\xi \quad (3)$$

where $\Phi_{J'J''}$ is the molecular transition lineshape function, g is the spectral distribution of the excitation laser convolved by the same profile, $\sigma_{J'J''}$ is the transition J'J'' wavenumber and σ_L is the laser wavenumber . Fluorescence quantum yield is expressed as:

$$\Phi(T,P) = \frac{A_{v'v''}}{\sum_{v''} A_{v'v''} + Q + P + W_i} \quad (4)$$

where v', v'' refer to the vibrational quantum numbers in upper and lower states, respectively, $A_{v''v'}$ is the Einstein coefficient for spontaneous emission for a given vibrational (v'-v'') transition (s^{-1}), Q the collisional quenching rate (s^{-1}), P the predissociation rate (s^{-1}) and W_i the ionisation rate (s^{-1}) due to the absorption of a third photon.

II.2. Excitation spectrum

In order to have a versatile tool capable of simulating CO excitation spectra for various thermodynamic conditions, we have considered the following free input parameters: temperature, pressure, chemical composition of the gas phase, wavelength scanning range, laser linewidth and laser intensity. By contrast, all spectroscopic data (quenching cross section, broadening coefficient…) are stored hard in matrices. Experimental parameters η and Ω in Eq. 1 are fixed equal to 1 in our simulation code. The transmission curve of the filters used for fluorescence detection is included in our code, as experimental results in our previous article [4] showed its importance on the shape of the excitation spectra.

Two-photon excitation spectra of A(v'=0-5)-X(v''=0), B(v'=0)-X(v''=0) and C(v'=0)-X(v''=0) transitions are simulated using Eq (1). The first step consists on calculating the spectral position of each rotational line. The rotational energies of states $X^1\Sigma^+(v''=0)$, $B^1\Sigma^+(v'=0)$ and $C^1\Sigma^+(v'=0)$ are calculated using classical formulae for $^1\Sigma^+$ state [16] and the spectroscopic constants reported in Table 1, that are deduced from Varberg and Evenson [16] for the ground state and from Amiot et al. [17] for the excited states. For the $A^1\Pi(v'=0\text{-}5)$ state, we used the values given by Le Floch [18], who takes into account perturbations of Λ-doubling due to different interactions with adjacent singlet or triplet states. The rotational energies of each electronic state are stored in matrices. Then, the lines positions of both B(v'=0,J')-X(v''=0,J'') and C(v'=0,J')-X(v''=0,J'') systems are determined by following the two-photon selection rules for $^1\Sigma^+$-$^1\Sigma^+$ transition ($\Delta J=0, \pm 2$), yielding to three branches (S, Q and O) for each rotational level J''. For the $A^1\Pi(v'=0\text{-}5,J')$-$X^1\Sigma^+(v''=0,J'')$ transition, two-photon selection rules ($\Delta J=0, \pm 1, \pm 2$) lead to five branches (S, R, Q, P and O).

Intensity of each rotational line is calculated from Eq. 1. For B-X transition, the two-photon absorption cross-section $\sigma_{v'',v'}$ (electronic and vibrational part in cm^4) is taken from Di Rosa and Farrow [19]. No measurements of the two-photon cross section are available for C-X and A-X transitions in the literature. The fractional population in the $X^1\Sigma^+(v''=0, J'')$ is calculated considering the classical

Maxwell-Boltzmann distribution law. The two-photon Hönl-London factors for linear polarization are given by Bray and Hochstrasser [20] for the two types of transition, namely, $^1\Sigma^+$-$^1\Sigma^+$ and $^1\Pi$-$^1\Sigma^+$.

For the $^1\Sigma^+$-$^1\Sigma^+$ transition, Hönl-London factors for S, Q and O branches are written as:

$$S_O^{(2)} = \frac{J''(J''-1)}{30(2J''+1)}\mu_S^2 \tag{5}$$

$$S_Q^{(2)} = \frac{2J''+1}{9}\mu_I^2 + \frac{2J''+1}{45(2J''+1)(2J''+3)}\mu_S^2 \tag{6}$$

$$S_S^{(2)} = \frac{(J''+1)(J''+2)}{30(2J''-1)}\mu_S^2 \tag{7}$$

where μ_I^2 and μ_S^2 are the transition dipole factors for linear and circular polarization [20], that are not available in the literature. Nonetheless, these parameters can be estimated experimentally from the polarization ratio given by:

$$\frac{\sigma_{ll}}{\sigma_{cc}} = \frac{2}{3}\left(1+\frac{5(2J''+3)(2J''-1)\mu_I^2}{2J''(J''+1)\mu_S^2}\right) \approx \lim_{J''\to\infty}\frac{2}{3}\left(1+10\frac{\mu_I^2}{\mu_S^2}\right) \tag{8}$$

For B-X transition, Tjossem et al. [21] indicate that $\sigma_{ll}/\sigma_{cc} \geq 200$ in the limit of large J'', which yields $\mu_I^{2/}\mu_S^2 \geq 30$. Consequently, the second term in Eq. 6 can be neglected and the ratio S(J'')/2J''+1 becomes independent of the rotational quantum number J''. Furthermore, Hönl-London factors for the S and O branches are lower than that of the Q branch by at least a factor of 30. Similarly to Linow et al. [2], we apply the same formalism for the C state.

For the $^1\Pi$-$^1\Sigma^+$ transition and linear polarization, Hönl-London factors are given by:

$$S^O(J'') = \frac{J''(J''+2)}{15(2J''-1)}\mu \tag{9}$$

$$S^P(J'') = \frac{(J''+1)^2}{30(J''-1)}\mu \tag{10}$$

$$S^Q(J'') = \frac{(2J''+1)}{10(2J''-1)(J''+3)}\mu \tag{11}$$

$$S^R(J'') = \frac{J''}{30}\mu \tag{12}$$

$$S^S(J'') = \frac{(J''+1)(J''+3)}{15(2J''+3)}\mu \tag{13}$$

where μ is the transition dipole factor for each branch. Without values in the literature, we used μ=1 in our simulations, which yields good comparison with the experimental spectra of Mosburger et al. [5].

Fluorescence quantum yield is calculated by using Eq. 4, where Einstein coefficients $A_{v'',v'}$ for B-A and A-X transitions are taken from [22]. For the Herzberg band (C-A), the emission probabilities for different vibrational transitions are simply given by the Franck-Condon factors [23], due to the lack of $A_{v'',v'}$ values. In Eq. 4, collisional quenching rate is calculated from the expression $Q(T,P) = \sum_i N_i \bar{v}_i \sigma_Q^i(T)$, where N_i is the number density of the quencher i; $\bar{v}_i$ is the relative velocity and $\sigma_i(T)$ is the temperature-dependent quenching cross-section. Collisional quenching of the B state has been investigated in details [24-28]. In particular, the temperature-dependent quenching cross-sections of CO B(v'=0) state were measured by Settersten et al. [28], at temperatures between 293 K and 1031 K (see Table 2) for all major species in combustion (N_2, O_2, CH_4, CO, CO_2, H_2O). No rotational dependence of the quenching cross-section was reported by these authors who deduced for each colliding species a power-law for the temperature dependence of the quenching cross-section:

$$\sigma_Q^i(T) = \sigma_0^i\left(\frac{T}{293}\right)^{n_i} \tag{14}$$

where σ_0^i is the quenching cross-section of species i at 293 K and n_i the temperature exponent. Quenching cross-section and coefficients n_i are reported in Table 2. Quenching cross-sections for the A state taken from [29, 30] are also reported in Table 2 for a limited number of colliders. No temperature-dependence of quenching cross-section is available though. For the C state, data are missing in the literature. Nonetheless, a much larger dipole moment (4.5 Debye for the C state as opposed to 1.85 Debye for the B state) indicates a larger quenching cross-section due to strong dipole / dipole or dipole / induced-dipole interactions. This was verified by Rosell et al. [3] who have reported

a much larger signal decrease with pressure for the Herzberg band (C-A) than for the Angström band (B-A). Finally, ionisation rate W_i is given by:

$$W_i = \sigma_i \left(\frac{I_L}{h\upsilon} \right) \tag{15}$$

where σ_i (cm^2) is the ionisation cross-section, I_L the laser intensity, h the Planck constant (6.62×10^{-34} J.s) and ν the laser frequency. Ionisation cross-section due to three-photon absorption at 230.1 nm (B-X scheme) has been determined experimentally to be equal to $1\pm0.3\times10^{17}$ cm^2 by Di Rosa and Farrow [31] and 0.7×10^{17} cm^2 by Looney et al. [32]. A J-dependency of the ionisation cross-section has been highlighted by Di Rosa and Farrow [31] for J=0-8 and 12, while Voigt et al. [8] provide information for J=9-11. These values have been included in our model. No data is available for the C state in the literature. Nonetheless, similarly to Linow et al. [2] the ionisation cross-section of the B state is used for the C state as well. For the A(4)-X(0) transition, the probability of ionisation is smaller, because it requires the absorption of four photons at 283.7 nm (141000 cm^{-1}) to exceed the ionisation threshold (113000 cm^{-1}). Consequently, ionisation efficiency can be neglected in the fluorescence quantum yield. Predissociation of the B(v'=0) state occurs for J'>37, with a rate of the same order as the radiative decay rate 10^7 s^{-1} [21]. By contrast, ionisation rate is equal to 1.2×10^9 s^{-1} for I_L=0.1 $GW.cm^{-2}$ and quenching rate is in the order of 10^9 s^{-1} in flames at 0.1 MPa, and thus predissociation rate can be neglected. For the $C^1\Sigma^+$(v'=0) state, no predissociation has been reported by Amiot et al. [17]. Finally, the energy of the $A^1\Pi$(v'=4) state of 70467,5285 cm^{-1} [18] is much lower than the dissociation limit (89 592 cm^{-1} [33]), so that no predissociation has to be considered.

Additionally, the distribution of rotational lines intensities is corrected for the transmission of the bandpass filter used for fluorescence detection in our previous article [4].

Finally, the transition lineshape is calculated using a Voigt algorithm [34], resulting in the convolution between Gaussian (Doppler) and Lorentzian (natural and collisional broadening) profiles. Transition lineshape is then convolved with the two-photon laser lineshape, that is assumed to be Gaussian and expressed as:

$$g(2\sigma_L) = \frac{2}{\Delta\sigma_L}\sqrt{\frac{\ln(2)}{2\pi}}\exp\left[-4\ln(2)\left(\frac{2\sigma_L - 2\sigma_{L,0}}{\sqrt{2}\Delta\sigma_L}\right)^2\right] \quad (16)$$

where $\Delta\sigma_L$ is the full width at half-maximum (FWHM) of the laser line (cm^{-1}), σ_L is the laser wavenumber (cm^{-1}) and $\sigma_{L,0}$ is the laser centre wavenumber (cm^{-1}). Note that for the case of a two-photon process, g (2σ) is $\sqrt{2}$ larger than for the case of a single photon process. The value of $\Delta\sigma_L$ is a free input parameter in our simulation code. Molecular lines are only broadened by Doppler and pressure effects. Natural broadening of the order of 10^{-4}-10^{-3} cm^{-1} is negligible in our temperature and pressure conditions. The Doppler width is equal to $2\sigma_{J'J''}(2kT\ln(2)/m_{co}c^2)^{1/2}$; where $\sigma_{J'J''}$ is the transition wavenumber (cm^{-1}), k the Boltzmann constant (1.38×10^{-23} $J.K^{-1}$), m_{co} the mass of CO molecule (4.65×10^{-26} kg) and c the speed of light (3×10^{8} $m.s^{-1}$). Assuming the impact approximation (and for a binary collision) [35], collisional width, $\Delta\sigma_c$ and collisional shift, $\Delta\sigma_s$ are calculated with classical laws:

$$\Delta\sigma_C = P\sum_i X_i 2\gamma_i \quad (17)$$

and,

$$\Delta\sigma_S = P\sum_i X_i \delta_i \quad (18)$$

where P is the total pressure (atm), X_i the molar fraction of the species i in the mixture, $2\gamma_i$ the broadening coefficient of the species i per pressure unit ($cm^{-1}.atm^{-1}$) and δ_i the shift coefficient of the species i per pressure unit ($cm^{-1}.atm^{-1}$). The temperature dependence of $2\gamma_i$ and δ_i is described by a power law:

$$2\gamma_i = 2\gamma_i^{T_0}\left(\frac{T_0}{T}\right)^{m_i} \quad (19)$$

and,

$$\delta_i = \delta_i^{T_0}\left(\frac{T_0}{T}\right)^{n_i} \quad (20)$$

where $2\gamma_i^{T_0}$ and $\delta_i^{T_0}$ correspond to the values of broadening and shift coefficient at T_0, m_i and n_i the temperature exponent. Shift-to-width ratio ($\delta/2\gamma$) and temperature exponent depend on the nature of bi-molecular interactions. In the case of London dispersion forces [35], shift-to-width ratio is equal to -0.363 and n=0.7. The broadening (2γ) and shift (δ) coefficients and the temperature exponents (m and n) for the Q rotational lines in the B-X (0,0) band (see Table 3) are taken from Di Rosa and Farrow [6] who performed measurements between 295 and 1010 K, and pressure up to 50 kPa with N_2, CO_2, and CO as colliders. Broadening and shift coefficients are J-independent [6]. For the case of O_2 and H_2O, these collisional parameters are not available. Nonetheless, the value of dipole moment for N_2 and O_2 is similar, therefore, the N_2 broadening and shift coefficients are also used for O_2. For CO-H_2O collision, an analogy can be made with NO-H_2O. Indeed, the B-X transition of CO presents similar characteristics with the A-X transition of NO (γ transition). The values of the dipole moment of CO (X) and NO (X) are close to each other (0.1 and 0.15 Debye, respectively). Additionally, intermolecular forces strengths (London dispersion forces for slightly polar or non-polar colliders) are equivalent with the London dispersion coefficients C_6 of 80.7±6.9 a.u. for CO(X)-N_2 [36] and 73 a.u. [37] for NO(X)-N_2. Molecules with high polarity such as H_2O (1.85 Debye), lead to strong intermolecular interactions and consequently induces larger broadening and shift. For instance, Di Rosa and Hanson [37] indicate $2\gamma_{H_2O} = 1.3 \times 2\gamma_{N_2}$ and $\delta_{H_2O} = 1.3 \times \delta_{N_2}$ for NO(X)-H_2O collision. By analogy with NO, broadening and shift coefficient for CO-H_2O collision are estimated to be $0.97 \times (295/T)^{0.77}$ and $-0.29 \times (295/T)^{0.53}$, respectively.

For A-X transition, Ar-broadening and self-broadening coefficients are only known at 300 K with 2γ=0.14 $cm^{-1}.atm^{-1}$ (CO-Ar) [38] and 2γ=0.236±0.046 $cm^{-1}.atm^{-1}$ (CO-CO) [39] without J and v-dependencies. Since the values for other colliders (N_2, O_2, H_2O and CO_2) are not available in the literature, a mean value of the broadening coefficients equal to 0.2 $cm^{-1}.atm^{-1}$ at 300 K is assumed in this work. A $T^{0.7}$ power dependence for self-broadening has been reported by Stark and al. [39], indicating that London dispersion forces are the main source of collision dephasing [6]. Considering a shift-to-width ratio equal to -0.36 for London dispersion forces [35], the shift coefficient is estimated to be equal to 0.086 $cm^{-1}.atm^{-1}$.

Owing to the lack of collisional parameters for C-X transition, broadening and shift coefficients are respectively approximated to $1\times(300/T)^{0.7}$ and $-0.36\times(300/T)^{0.7}$ assuming London dispersion forces in the case of weakly or non-polar colliders, resulting in a satisfactory agreement with the excitation spectrum measured in flames by Linow et al. [2].

It is well known that strong laser intensities such as those used in two-photon excitation process induce broadened, shifted and asymmetric lineshapes due to Stark effect. For our laser intensities range [4] (i.e. $I_L \leq 0.2$ GW.cm^{-2}), Di Rosa and Farrow [32] report a Stark broadening and shift less than 0.01 cm^{-1} for B-X transition which are insignificant compared to collisional and Doppler broadening in our temperature and pressure conditions. On the other hand, very high laser intensity is required for two-photon excitation of A-X transition. For example, Mosburger and Sick [5] have used a laser density equal to 13 GW.cm^{-2} so that Stark broadening and shift are no longer negligible. Girard et al. [40] have observed a change of FHWM and shift approximately equal to 0.3 cm^{-1} for 15 GW.cm^{-2}. Accordingly, the Stark effect is taken into account for A-X transition, in our model. As mentioned by Di Rosa and Farrow [32], Stark shift is expressed as:

$$\Delta\sigma_s = \frac{2\pi\sigma_s}{hc\upsilon} I_L \tag{21}$$

where σ_s is the Stark shift cross-section, h the Plank constant, c the speed of light, ν the laser frequency and I_L the laser intensity. From measurements of Girard et al. [40], we deduced a Stark shift cross-section equal to 9×10^{-18} cm^2 and a variation of Stark broadening as $0.0248\times I_L$, with I_L the laser intensity in GW.cm^{-2}.

In our previous article [4], asymmetric profiles of the Q branch have been observed experimentally for pressure higher than 0.1 MPa at 300 K. This trend cannot be explained by a classical Voigt profile or other profiles taking into account particular effect due to collisions, such as Doppler narrowing (Galatry profile [41]) or thermal motion induced modifications of broadening width (Speed Dependent Voigt Profile [42]). As mentioned by Vyrodov et al. [43] for NO molecule, these low pressure theories

fail to describe asymmetric profile, because the main assumptions of these theories are binary and instantaneous collisions (impact approximation), that are no longer valid at high pressure. Indeed, collision duration is approximately of 1 ps for CO [41], whereas the time between two collisions is equal to 8 ps at 300 K and 1.3 MPa.

Another approach called statistical theory suited to high pressure regimes [44] is deduced from statistical distribution of frequency perturbations. It assumes that perturbing molecules are fixed around the emitting molecule in low temperature and high pressure environment. Considering London dispersion forces, Margenau and Watson [44] obtained a red shift of spectral line in the same direction as asymmetry. In addition, this theory leads to collisional broadening and shift proportional to P^2, that are not compatible with the shift measurement reported in [4], where the shift was in the form $aP+bP^2$. Moreover, statistical behaviour was only observed for atomic spectra measured at several tens of atmospheres [44].

Therefore, the use of generalized pressure theories [45, 46], that are valid in a wide range of pressures, is believed to be more appropriate for our spectral simulation purposes. For example, the Lindholm profile gives a good agreement for NO [43] and O_2 [47] molecules at pressure up to 0.5 and 6.0 MPa, respectively. The Lindholm theory [45] is the first attempt to unify impact approximation (Lorentz profile) at low pressure and statistical theory at high pressure, including time collision which leads to an asymmetric profile. This model is based on Fourier transform approach for correlation dipole moment function. The Lindholm model is confined to Van der Waals interactions (long-range interaction), by contrast to the Anderson model which includes interaction through a series expansion beginning by dipole-dipole interaction ($1/R^3$) [46]. The Lindholm model assumes that: 1) all colliders possess the same velocity relative to the emitter and let this velocity to be the relative mean velocity, 2) collider travels in straight lines, 3) collisions are adiabatic. This model leads to an asymmetric profile with a frequency dependence of $1/\nu^{3/2}$ in the red wing and $1/\nu^{7/2}$ in the blue wing. The Lindholm theory has been verified experimentally for sodium lines broadened by argon [48]. The Lindholm profile is defined by:

$$I(\upsilon) = I_0 + I_\infty \tag{22}$$

with,

$$I_0 = \int_0^1 \exp\left[-l(0.369y^{4/3} + 0.591y^{1/2}) \times \cos(ky + l(0.369y^{4/3} + 0.591y^{1/2})\right]dy \quad (23)$$

and,

$$I_\infty = \exp\left[-0.960l\right] \times \left[\frac{0.795l\cos(0.804l+k) - (k+0.577l)\sin(0.804l+k)}{(0.795l)^2 + (k+0.577l)^2}\right] \quad (24)$$

with

$$k = (\upsilon - \upsilon_0)\frac{4\pi x}{\bar{v}}\left(\frac{3\pi\Delta C_6}{h\bar{v}}\right)^{1/5} \quad (25)$$

and,

$$l = N4\pi x\left(\frac{3\pi\Delta C_6}{h\bar{v}}\right)^{3/5} \quad (26)$$

where x=1.7 (this value allows to obtain a perfect agreement with statistical theory at high pressure), $\bar{v}$ is the mean relative velocity ($m.s^{-1}$), ΔC_6 the difference of London dispersion coefficient (ΔC_6= C_6(upper state)-C_6(lower state), $J.m^6$). By contrast, with the Voigt profile, broadening, shift and asymmetry are correlated and given by Eq. 26.

From Eqs. 22-26, an algorithm for the Lindholm profile has been developed and included in our simulation code. For spectral line shape calculation, input parameters are C_6 coefficients for the ground state $X^1\Sigma^+$ and the $B^1\Sigma^+$ state. For X state, Parker et al. [36] indicate C_6=80.7±6.9 a.u. for CO-N_2, 62.8±3.3 a.u. for CO-O_2, 128.6±8.7 a.u. for CO-CO_2 and 88.4±9.7 a.u. for CO-CO. For B state, Di Rosa and Farrow [6] have shown that C_6 coefficients for CO-CO and CO-N2 collisions at 295 K are approximately 1.7 times larger than C_6 values for NO(A)-NO and NO(A)-N_2 at 295 K [37]. Hence, we obtain C_6=651.1 a.u. for CO(B)-N_2 and C_6=589.9 a.u. for CO(B)-CO. C_6 coefficients for CO (X) state can be neglected in Eqs. 23 and 24 because they are an order of magnitude smaller than the ones for CO(B) state. In our simulation, we consider only C_6 coefficient for CO-N_2 because of 1) the lack of experimental data for validation, 2) our measurements for validation were performed for a mixture composed of 2.6 % of CO in air [4]. The Lindholm profile is also convolved by laser lineshape, that is assumed to be Gaussian and calculated according to Eq. 16.

Excitation spectrum is the result of the sum of each rotational line, where line-mixing phenomena are not taken into account. Owing to the lack of spectroscopic constants for C-X and A-X transition, only the distribution of rotational line intensity with temperature (Boltzmann distribution) is calculated.

II.3. Fluorescence spectra

Similarly to the excitation spectra, the free input parameter for modelling fluorescence spectra are: temperature, pressure, chemical composition of the gas phase, excitation wavelength, spectrometer resolution, laser linewidth and laser intensity. Experimental parameters η and Ω are fixed equal to 1.

Dispersed fluorescence spectrum (one-photon) is also computed with Eq. 1 for A(v'=0-5)-X(v''=11-15), B(v'=0)-A(v''=0-5) and C(v'=0)-A(v''=0-5) bands. Firstly, rotational levels involved in the laser excitation are calculated together with their intensity. From rotational energies, the lines positions of these three bands are calculated using one-photon selection rules for $^1\Sigma^+$ - $^1\Pi$ transition ($\Delta J=0, \pm 1$) which lead to 3 branches P, Q and R. The lines position of A-X are calculated using one-photon selection rule for $^1\Pi$-$^1\Sigma^+$, which leads to 3 branches, namely P, Q and R. Rotational line strengths are calculated by using the Hönl-London factors for $^1\Sigma^+$ - $^1\Pi$ and $^1\Pi$-$^1\Sigma^+$ transitions [49]. The fluorescence lineshape is calculated using the Voigt algorithm [34], and is mainly broadened by the spectrometer instrumental profile (Gaussian profile with FWHM=1 nm). The collisional width for each rotational line is selected to be $0.1(300/T(K))^{0.5}$.

Example of fluorescence spectrum calculation is presented in Fig. 2. Comparison with experimental results shows that the position, amplitude and the width of the different vibrational bands are well reproduced by the simulations. Disagreement at 560 and 607 nm is due to the reduced sensitivity of the ICCD camera above 560 nm where the quantum efficiency of the intensifier is below 5 %.

III. Results

This section presents a comparison between measurements and simulations of CO fluorescence for various thermodynamic conditions. Experimental data are taken from [4] and details about the experimental set-up and processing methods are recalled in the first part of the section. In short, two-photon fluorescence signals from CO molecule were measured as a function of laser intensity, temperature (300 to 900 K), pressure (0.1 to 1.3 MPa), CO concentration (0.33 to 2.6% of CO in air) in a high-temperature / high-pressure test cell and in a laminar premixed methane/air flame. The second part of the section investigates the influence of temperature on LIF spectra (excitation and dispersed fluorescence). In the third part of the section, the effect of pressure on LIF spectra is determined and comparison between experiments and simulations highlights the limitations of the classical Voigt lineshape modelling as pressure increases. The Lindholm profile is subsequently applied and a better agreement with experiments at elevated pressure is demonstrated.

III.1. Experimental setup

The experimental investigations are carried out in a high pressure cell (pressure range from 0.1 to 1.3 MPa) equipped with optical ports for LIF diagnostics. The cell is made of stainless steel and designed for operating in the temperature range from 300 to 900 K with CO and synthetic air (80 % N_2 and 20 % O_2 in molar fraction). Mass flow controllers (Bronkhorst) are used to regulate the gas flow rates (0.008 L/min for CO and 0.3 L/min for air). The molar fraction of CO in the CO/air mixture is thus equal to 2.6 %. The exits of the flowmeters are connected to a premixing duct (ensuring full premixing between CO and air) which outlet is connected to the cell. Temperature of the gas inside the cell is controlled by means of a type K thermocouple placed a few millimetres aside of the laser probe volume. Temperature values mentioned in Figs. 2-8 correspond to the gas temperature measured by this thermocouple. The pressure is measured with a pressure transducer (Tb244, JPB). Windows are made of UV fused silica (7980 KrF grade, Corning). Two windows are used for laser beam access, while fluorescence light is collected through a third window placed at 90° from the laser beam axis. In the flame experiments, the test cell is replaced by a water-cooled porous burner (diameter: 19 mm)

generating a laminar premixed CH_4/air flat flame. Flow rates are equal to 0.22 L/min for CH_4 and 1.80 L/min for air, leading to an equivalence ratio of 1.16.

Generation of a laser beam at 230.1 nm (excitation of the $B^1\Sigma^+ \leftarrow X^1\Sigma^+$ (0,0) band) is obtained using the second harmonic of the Nd:YAG laser (YG781, Quantel) at 532 nm to pump a tuneable narrow-linewidth dye laser (TDL50, Quantel) which operates with Rhodamine 610. The fundamental dye laser is frequency-doubled with a KD*P crystal. The resulting 293 nm beam is then frequency-summed with the residual of the YAG fundamental (at 1064 nm) using a mixing crystal to deliver a beam at 230.1 nm. The pulse duration is 6 ns, the energy is 1 mJ/pulse and the linewidth is equal to 0.7 cm^{-1}. Let us note that this is a theoretical value of the laser linewidth which could not be measured for the beam at 230.1 nm by our wavelength meter (WS6-600 VIS Standard, HighFinesse). Nonetheless, we have verified that the linewidth of the beam at 1064 nm is indeed equal to 0.7 cm^{-1}. At the laser system exit, the laser beam is transported to the test cell (or to the flame) by means of mirrors. The beam is focused using a spherical UV lens (focal length: 500 mm), which leads to an estimated diameter of 190 µm at the probe volume. All of the results displayed in this paper have been obtained for a laser energy reduced to 0.4 mJ/pulse (power density of 0.2 GW/cm^2), in order to ensure a quadratic dependence of the 2-photon LIF signal upon laser intensity whatever the experimental conditions and also to limit the ionisation of CO molecules. Laser energy is recorded shot-to-shot by means of a photodiode (DET210, Thorlabs) in order to correct fluorescence signals for the temporal fluctuations of the laser pulses. For recording LIF excitation spectra, laser wavelength is scanned around 230 nm in 0.3 pm steps, over 226 pm (at 300 K, 0.1 MPa) and 470 pm (at 900 K, 1.3 MPa). For recording dispersed fluorescence spectra, the laser wavelength is first tuned to the peak of the excitation spectrum (around 230.105 nm) for each thermodynamic condition.

For excitation spectra measurements, fluorescence light is collected at right angle by a spherical UV lens (diameter: 50 mm, focal length: 100 mm) and imaged with a magnification of 1 onto a pinhole (diameter: 2.5 mm) placed in front of a photomultiplier tube. Spectral filtering of the fluorescence is performed with a bandpass filter centred at 485 nm with a full width at half maximum (FWHM) of 25

nm and a transmittance larger than 92%. The filter is placed between the pinhole and the photomultiplier and allows to record fluorescence from the B(0)-A(1) band around 483 nm. For each laser wavelength of the scanning range, the output signal from the photomultiplier is time-integrated (over 15 ns) and averaged over 30 laser shots by a Boxcar system. A Labview® interface is used to acquire both integrated photodiode ~~signal~~ and integrated fluorescence signals and display the spectra. For recording dispersed fluorescence spectra, fluorescence is collected at right angle by two spherical UV lenses (diameter: 50 mm, respective focal length: 160 and 100 mm), which image the probe volume onto the entrance slit (height: 150 μm, width: 15 mm) of a spectrograph (SPEX270M, Jobin-Yvon). The slit is oriented parallel to the laser axis, so that light collection is spatially integrated over 15 mm. The grating of the spectrograph is blazed at 400 nm with 600 groves/mm. The light dispersed by the grating is recorded using a 16-bit intensified CCD camera with an intensifier gate width of 500 ns. The CCD array is 576 × 384 pixels and the framing rate of the system is fixed to 10 Hz by using full binning over the 384 pixels. The collected light is dispersed over the CCD width (576 pixels), corresponding to a spectral range of 80 nm and a resolution of 0.138 nm/pixel. The ICCD camera is interfaced to a personal computer which is used to control the camera and acquire the spectra. The spectral resolution of the detection system is about 1 nm, which is not enough to distinguish the fine rotational structures in the fluorescence spectrum at ambient temperature. For each experimental condition, fluorescence measurements are averaged over 1000 laser shots. Each dispersed fluorescence spectrum and each excitation spectrum is corrected for beam attenuation due to absorption. All of the results given in this article are referenced to the same molar fraction of CO (i.e. 2.6 %) because flow rates of CO and air are kept constant for all experiments. After recording a fluorescence spectrum, an equivalent set of measurements is also acquired immediately with the same laser energy in the cell evacuated from any CO to allow subtraction of stray and scattered light from fluorescence signals. Spectra are corrected for the spectral response of the detection system using calibration from the emission continuum of a deuterium lamp. Temperature, pressure and CO/air molar fraction are thoroughly controlled and measurements are performed in steady state conditions.

III.2. Influence of temperature on LIF spectra

A comparison between simulated and experimental excitation spectra at 300, 600, 860 and 1750 K (in a flame) and 0.1 MPa is presented in Fig. 3. A good agreement is obtained between experiments and simulation (both with Voigt and Lindholm profiles) for each temperature. In particular, the shape and the width of the excitation spectrum are well reproduced by the simulations. Indeed, at 300 K, the width of the spectrum at half intensity is 3.83 cm^{-1} in experiments, 3.73 cm^{-1} with the Voigt profile and 3.69 cm^{-1} with the Lindholm profile. However, the Voigt profile fails to reproduce excitation spectrum towards lower energy (red wing), contrary to the Lindholm profile. A slight disagreement of about 3% is noted in the red wing with the Voigt profile. Nonetheless, agreement improves as temperature increases, above 600 K, both Voigt and Lindholm profiles are suitable to reproduce the red wing and the amplitude of the spectral lines. Nonetheless, the rotational lines are not completely resolved at 860 K between 86925 and 86930 cm^{-1}, which may be due to the use of a too wide laser spectral profile for the simulations (see below). In the CH_4/air flat flame, the best fit with a Voigt profile is obtained for 1750±50 K (in agreement with combustion modelling [50-52]), by adjusting the temperature to match the rotational structure which is relatively well resolved in the blue wing (for J>24). Simulation at 1850 K overestimates the line intensity by 8% and underestimates it by 5% at 1650 K. Gas phase composition used for spectra simulation in the CH_4/air flame was taken from calculations with the Chemkin package (78% N_2, 10% H_2O, 8% CO_2 and 4% CO) [50-52]. It is noted that the best fit of the Q-lines is obtained for a laser linewidth of 0.8 cm^{-1}, that is 0.1 cm^{-1} larger than the value given by the laser manufacturer (Quantel). Indeed, by using a laser linewidth of 0.7 cm^{-1}, each CO line intensity is overestimated by 5%. In the simulation code, we preferred to privilege an accurate description of each CO line intensity by using a laser linewidth of 0.8 cm^{-1}, although slightly detrimental to the spectral resolution. As mentioned in [4], the hole observed at 86916 cm^{-1} (Fig. 3(d)) is attributed to the $P_1(8)$ line of the $B^2\Sigma^+(v'=0)\leftarrow X^2\Sigma^+(v''=1)$ transition of CO^+ ions [53], which coincides with the Q(9) line of CO ($B^1\Sigma^+(v'=0)\leftarrow X^1\Sigma^+(v''=0)$). This leads to a higher ionisation cross-section, as mentioned by Voigt et al. [8]. This feature is well reproduced in our calculated spectra by using the J-dependency of the ionisation cross-section proposed by Di Rosa and Farrow [32] and Voigt et al. [8].

Experimental and simulated variations of the integrated fluorescence spectra with temperature at 0.1 MPa are also shown in Fig. 4. Measurements are in relatively good agreement with simulation except

at 400 and 700 K where disagreements, which are attributed to laser instabilities due to high temperature in the laboratory cause by the high-temperature cell, are observed.

III.3. Influence of pressure on LIF spectra

Figures 5 and 6 present comparisons between experimental and simulated spectra (Voigt and Lindholm profiles) for several temperatures and pressures. Simulations with the Voigt profile were performed with experimentally-deduced shifts [4]. With the Voigt profile, the maximum of the excitation spectrum is in good agreement with experiments regardless pressure and temperature. At 300 K, simulations fail to reproduce the shape of the experimental spectrum that is asymmetric, whereas the Voigt profile leads to a quasi-symmetric shape at high pressure, in particular at 1.3 MPa. By contrast, the Lindholm profile provides a satisfying representation for shift, and shape up to 0.5 MPa. For pressure higher than 0.5 MPa, the red wing (lowest energy) of the spectrum is systematically overestimated by the Lindholm simulation, and disagreement increases with pressure; residual for the red wing increases by a factor of 2 between 0.7 and 1.3 MPa. At 860 K, the Voigt profile gives a satisfactory representation of red wing, while blue wing (highest energy) is overestimated. A relative good agreement is obtained with the Lindholm simulation for pressure up to 0.7 MPa Beyond 0.7 MPa, the red wing is once again overestimated in simulations, however, the residual is smaller than that at 300 K. This is due to the fact that asymmetry decreases as temperature increases.

The evolution of collisional shift simulated with the Lindholm profile at 300 and 860 K is presented in Fig. 7. The experimental shift is deduced from the difference between the position of the maximum of the Q branch and the Q(5) line at 86 916.918 cm^{-1}. The calculated shift is deduced from an individual line (J=6). At 300 K, a similar trend is obtained with a collisional shift expressed as $-\Delta\sigma_S=2.37\times P+1.27\times P^2$. For pressure lower than 0.1 MPa, simulations match the values of Di Rosa and Farrow [6], because at low pressure the Lindholm theory converges to impact approximation. At 860 K, the shift becomes linear with pressure up to 1.0 MPa, due to the decrease of collisional shift with temperature. Indeed, calculated values are equivalent to those of Di Rosa and Farrow [6] that are extrapolated at high pressure. Disagreement between simulation and experiment can be explained by

the fact that the shift is measured at the maximum of the Q branch, by contrast to the simulation, where the shift is calculated on a single line.

Figure 8 shows the variation of the maximum of the Q branch with pressure at 300 and 860 K. At 300 K, the variation of LIF signal with pressure is well reproduced by simulation. Between 0.1 and 1.3 MPa, LIF signal decreases by a factor of 2.7 for simulation and 3.1 for measurement. Slight disagreement corresponds to the measurement uncertainty equal to 10 % [4]. At 860 K, the variation is well reproduced up to 0.5 MPa and underestimated by 20 and 15 % at 1.0 and 1.3 MPa, respectively.

III.4. Discussion

Increasing temperature induces a reduction of the asymmetry lineshape of the Q branch and of the P^2 term in shift (Fig. 6). Moreover, simulations with Voigt and Lindholm profiles become similar when increasing temperature. These observations are due to the smaller density at higher temperature and a reduction of asymmetry as velocity increases with temperature. For NO molecule, Vyrodov et al. [54] report that simulations with Voigt and Lindholm profiles are similar in flames for pressure up to 3 MPa. By analogy, we can speculate that Voigt profile may be suitable to simulate excitation spectra in flames at high pressure. However, C_6 coefficients for CO (B) are approximately 1.7 times greater than C_6 for NO(A), which leads to broadening and shift 30% higher than for NO molecule [37]. The range of validity for CO is then potentially reduced to 0.1-1.8 MPa range, but this hypothesis requires further experimental validation. In a recent study, Voigt et al. [8] have performed CO measurement in a burner for pressure higher than 0.1 MPa. In this study, a simulation code of two-photon excitation spectrum of CO including a Voigt profile (validated for pressure up to 0.5 MPa) is used for calibration purpose [8]. Comparison between our simulation and the experimental spectrum of Voigt et al. [8] at 0.5 MPa has been performed. A good agreement with both Voigt and Lindholm profiles is obtained. However, the Lindholm profile slightly overestimates the red wings of Q branch. It is concluded that for future application in high-pressure flames typical of aircraft combustor (T~2000 K and pressure in the range 0.5-1.0 MPa), a Voigt profile together with collisional broadening and shift coefficient from DiRosa and Farrow [6] are well adapted to predict the behaviour of Q branch lineshape. Validity domain of Voigt and Lindholm profiles is resumed in Table 4.

In this study, we show that the Lindholm profile yields satisfactory agreement for pressure lower than 0.5 MPa and fails to reproduce the behaviour of the red wing for pressure higher than 0.5 MPa at 300 K. In our simulation, we assume that spectral lines are isolated from each other (no line mixing phenomena). This assumption involves that the energy difference between two lines is higher than collisional broadening ($|E_2 - E_1| >> \Delta\sigma_c$). However, the CO Q-branch contains a high density of lines in a limited spectral range, especially in the red wing (lower J), and collisional broadening is important. At 300 K and 0.1 MPa collisional broadening is equal to 0.7 cm^{-1}, whereas the difference between Q(0) and Q(1) lines is equal to 0.052 cm^{-1}. It is, therefore, obvious that these lines overlap, and line mixing would likely occur [41]. Line mixing phenomenon leads to a narrowing of the wings of a profile composed of overlapping lines [41], which can explain the difference between experiments and the Lindholm simulation at high pressure. Thus, it could be interesting to apply another theoretical approach that combines both line mixing and collision-time asymmetry (like the Lindholm theory) such as that developed by Ciuryło and Szudy [55].

IV. Conclusion

A versatile numerical code has been developed to calculate two-photon CO-LIF spectra in the ns regime over a wide range of thermodynamic conditions and chemical composition of the phase gas, for three excitation/fluorescence schemes (A-X/A-X, B-X/B-A and C-X/C-A). Our model including up-to-date spectroscopic constants is based on the following considerations:

1) A 5, 4 and 3-level model was used to simulate fluorescence and excitation spectra of A-X/A-X, B-X/B-A and C-X/C-A schemes, respectively;
2) Absorption line shapes are modelled with the Voigt profile. Doppler and collisional broadening and collisional shift are considered. Stark effect is also incorporated for the A state;
3) Line mixing is not considered;
4) Fluorescence occurs from a single vibronic excited state toward all the rovibronic levels possible of a low-lying excited state;

5) Non-radiative (quenching) and radiative (ionisation, except for A-X/A-X scheme) depopulation mechanism of the excited state are considered;
6) Predissociation is neglected for all excited states.

Simulations are more accurate for the B-X/B-A scheme, due to the lack of spectroscopic data for the other schemes. Temperature effect is well reproduced by simulations. Comparison between measured and simulated excitation spectra lead to a flame temperature of 1750 ± 50 K, in agreement with combustion simulations. Furthermore, experiments at high pressure show a strong asymmetry of the excitation spectra that is not reproduced by a Voigt profile. In order to capture this asymmetry, we used the Lindholm profile, which leads to a good agreement with experiments in the range 0.1 - 0.5 MPa at 300 K, and 0.1 - 0.7 MPa at 860 K. Nonetheless, the decrease of asymmetry with temperature suggests that a Voigt profile may be appropriate for high-pressure flames, as mentioned by Vyrodov et al. [44] for NO molecule. As such, it would be necessary to perform measurements in high-pressure flames in order to validate this hypothesis for CO molecule. Moreover, it would be interesting for future investigations to consider another theory in order to obtain a complete validation in a wide range of pressures and temperatures. The theory developed by Ciuryło and Szudy [50] seems to be very interesting, because mixing effect due to overlapping lines (as it is the case for CO molecule) and collision-time asymmetry are included.

Acknowledgements

Mr. O. Carrivain was supported by a PhD grant from ONERA.

REFERENCES

[1] J.M. Seitzman, J. Haumann, R.K. Hanson. "Quantitative two-photon LIF imaging of carbon monoxide in combustion gases". Appl. Opt. 1987. 26(14): 2892-2899.

[2] S. Linow, A. Dreizler, J. Janicka, E.P. Hassel. "Comparison of two-photon excitation schemes for CO detection in flames". Appl. Phys. B: Lasers Opt. 2000. 71(5): 689-696.

[3] J. Rosell, J. Sjöholm, M. Richter, M. Aldén. "Comparison of three schemes of two-photon laser-induced fluorescence for CO detection in flames". Appl. Spectrosc. 2013. 67(3): 314-320.

[4] O. Carrivain, M. Orain, N. Dorval, C. Morin, G. Legros. "Experimental spectroscopic Studies of Carbon Monoxide (CO) Fluorescence at High Temperatures and Pressures" Appl. Spectrosc. 2017. 71(10): 2353-2366.

[5] M. Mosburger, V. Sick. "Single laser detection of CO and OH via laser-induced fluorescence". Appl. Phys. B: Lasers Opt. 2010. 99(1): 1-6.

[6] M.D. Di Rosa, R.L. Farrow. "Temperature-dependent collisional broadening and shift of Q-branch transitions in the B←X(0,0) band of CO perturbed by N2, CO2 and CO" J. Quant. Spectrosc. Radiat. Transfer. 2001. 68(7): 363-375.

[7] L. Voigt, J. Heinze, T. Aumeier, T. Behrendt, F. di Mare, "Quantitative CO PLIF measurements in aeroengine gas turbine combustion chambers under realistic conditions" Proceedings of ASME Turbo Expo 2017: Turbomachinery Technical Conference and Exposition GT2017 June 26-30, 2017, Charlotte, NC, USA.

[8] L. Voigt, J. Heinze, M. Korkmaz, K.P. Geigle, C. Willert, "Planar measurements of CO concentrations in flames at atmospheric and elevated pressure by laser-induced fluorescence". Appl. Phys. B. 2019. 125:71.

[9] W. G. Bessler, C. Schulz, V. Sick, and J. W. Daily, A versatile modeling tool for nitric oxide LIF spectra, Proceedings of the Third Joint Meeting of the U.S. Sections of The Combustion Institute (Chicago, March 16-19, 2003, paper PI05), http://www.lifsim.com/.

[10] J. Luque, D.R. Crosley, "LIFBASE: Database and Spectral Simulation Program (Version 1.5)", SRI International Report MP 99-009 (1999).

[11] M. Ruchkina, P. Ding, M. Aldén, J. Bood, and C. Brackmann, "Two-photon-excited fluorescence of CO: experiments and modeling". Opt Express. 2019. 28(18): 25656-25668

[12] D.R. Richardson, S. Roy, and J.R. Gord, "Femtosecond, two-photon, planar laser-induced fluorescence of carbon monoxide in flames". Opt. Lett. 2017. 42(4): 875-878

[13] B. Li, X. Li, D. Zhang, Q. Gao, M. Yao, and Z. Li, "Comprehensive CO detection in flames using femtosecond two-photon laser-induced fluorescence". Opt. Express. 2017. 25(21): 25809-25818

[14] Y. Wang, and W.D. Kulatilaka, "Spectroscopic investigation of high-pressure femtosecond two-photon laser-induced fluorescence of carbon monoxide up to 20 bar". Appl. Opt. 2019. 58(10): 23-29

[15] O. Carrivain. "Etude de la spectroscopie LIF à deux photons de la molécule CO pour des mesures en flammes à haute pression". PhD Thesis. 2015. Université Pierre et Marie Curie, France.

[16] T.D. Varberg, K.M. Evenson. “Accurate far-infrared rotational frequencies of carbon monoxide” Astrophys. J. 1992. 385(1): 763-765.

[17] C. Amiot, J.Y. Roncin, J. Verges. “First observation of the CO $E^1\Pi \rightarrow B^1\Sigma^+$ and $C^1\Sigma^+ \rightarrow B^1\Sigma^+$ band systems. Predissociation in the $E^1\Pi$ (v = 0) level” J. Phys. B: At. Mol. Phys. 1986. 19(1): 19-23.

[18] A.C. Le Floch. “Etude des couplages rotationnels et spin-orbite dans l’état $A^1\Pi$ de la molécule CO”. PhD thesis. 1989. Université Paris-Sud, France.

[19] M.D. Di Rosa, R.L. Farrow. “Two-photon excitation cross section of the B←X(0,0) band of CO measured by direct absorption”. J. Opt. Soc. Am. B. 1999. 16(11): 1988-1994.

[20] R.G. Bray, R.M. Hochstrasser. “Two-photon absorption by rotating diatomic molecules”. Mol. Phys. 1976. 31(4): 1199-1211.

[21] P.J.H. Tjossem, K.C. Smyth. “Multiphoton excitation spectroscopy of the $B^1\Sigma^+$ and $C^1\Sigma^+$ Rydberg states of CO”. J. Chem. Phys. 1989. 91(4): 2041-2048.

[22] M. Lino Da Silva, M. Dudeck. “Arrays of radiative transition probabilities for CO_2-N_2 plasmas”. J. Quant. Spectrosc. Radiat. Transf. 2006. 102(3): 348-386.

[23] T.A. Carlson, N. Duric, P. Erman, M. Larsson. “Correlation between perturbation and collisional transfers in the A, B, C and b states of CO as revealed by high resolution lifetime measurements”. Z. Physik. A. 1978. 287(2): 123-136.

[24] F. Di Teodoro, J.E. Rehm, R.L. Farrow, P.H. Paul. “Collisional quenching of CO $B^1\Sigma^+$(v = 0) probed by two-photon laser-induced fluorescence using picosecond laser”. J. Chem. Phys. 2000. 113(8): 3046-3054.

[25] S.S. Dimov, C.R. Vidal. “Cross section for quenching of the CO $B^1\Sigma^+$ state in collisions with hydrogen and helium”. Chem. Phys. Lett. 1994. 221(3-4): 307-310.

[26] S. Agrup, M. Aldén. “Measurement of the collision-quenched lifetime of CO molecules in a flame at atmospheric pressure”. Chem. Phys. Lett. 1992. 189(3): 211-216.

[27] S. Agrup, M. Aldén. “Measurements of the collisionally quenched lifetime of CO in hydrocarbon flames”. Appl. Spectrosc. 1994. 48(9): 1118-1124.

[28] T.B. Settersten, A. Dreizler, R.L. Farrow. “Temperature- and species-dependent quenching of CO B probed by two-photon laser-induced fluorescence using a picosecond laser”. J. Chem. Phys. 2002. 117(7): 3173-3179.

[29] F.J. Comes, E.H. Fink. “Deactivation of CO ($A^1\Pi$) in individual vibrational levels”. Chem. Phys. Lett. 1972. 14(4), 433-436.

[30] L.A. Melton, K.C. Yiin. “Energy transfer in CO $A^1\Pi$, v’ = 9. I. Quenching and isotope effects” J. Chem. Phys. 1975. 62(11): 2860-2868.

[31] M.D. Di Rosa, R.L. Farrow. “Cross sections of photoionisation and ac Stark shift measured from Doppler-free B←X(0, 0) excitation spectra of CO”. J. Opt. Soc. Am. B. 1999. 16(5): 861-870.

[32] J.P. Looney, J.E. Harrington, K.C. Smyth, T.R. O'Brian, T.B. Lucatorto. "Measurement of CO pressures in the ultrahigh vacuum regime using resonance enhanced multiphotonionisation time-of-flight mass spectroscopy". J. Vac. Sci. Technol., A. 1993. 11(6): 3111-3120.

[33] M. Eidelsberg, J. Y. Roncin, A. Le Floch, F. Launay, C. Letzelter, J. Rostas. "Reinvestigation of the vacuum ultraviolet spectrum of CO and isotope species: The $B^1\Sigma^+ \leftrightarrow X^1\Sigma^+$ transition". J. Mol. Spectrosc. 1987. 121(2): 309-336.

[34] J. Humlicek. "An efficient method for evaluation of the complex probability function: the Voigt function and its derivates". J. Quant. Spectrosc. Radiat. Transfer. 1979. 21(4): 309-313.

[35] I.I. Sobelman, L.A. Vainshtein, E.A. Yukov. "Broadening of spectral lines". In: G. Ecker, I.I Sobel'man, P. Lambropoulos and H. Walther. Excitation of atoms and broadening of spectral lines. New York: Springer-Verlag Berlin Heidelberg, 1995. Vol. 15, Chap. 7, 237-296

[36] G.A. Parker, R.T. Pack. "Van der Waals interactions of carbon monoxide". 1976. J. Chem. Phys. 64(5): 2010-2012.

[37] M.D. Di Rosa, R.K. Hanson. "Collision broadening and shift of NO (0; 0) absorption lines by O_2 and H_2O at high temperature". J. Quant. Spectrosc. Radiat. Transfer. 1994. 52(5): 515-529.

[38] A. Jolly, J.L. Lemaire, D. Belle-Oudry, S. Edwards, D. Malmasson, A. Vient, F. Rostas. "High resolution 'VUV laser' measurement of the band oscillator strengths of CO $A^1\Pi$ ($9<v'<17$)-$X^1\Sigma^+$ ($v''=0$) transition". J. Phys. B: At. Mol. Opt. Phys. 1997. 30(19): 4315-4337.

[39] G. Stark, B.R. Lewis, S.T Gibson, J.P. England. "High-resolution oscillator strength measurements for high-v' bands of the $A^1\Pi$ (v')-$X^1\Sigma^+$ ($v''=0$) system of carbon monoxide". Astrophys. J. 1998. 505(1): 452-458.

[40] B. Girard, N. Billy, J. Vigue, J.C. Lehmann. "Evidence for a dynamical Stark effect in CO ($A^1\Pi$) two-photon excitation". Chem. Phys. Lett. 1983. 102(2-3): 168-173.

[41] J.M. Hartmann, C. Boulet, D. Robert. "General equations", Collisional effects on molecular spectra, Laboratory experiments and models, consequences for applications, Elsevier, 2008. Chap. 2, 47

[42] P.R. Bergman. "Speed-dependent collisional width and shift parameters in spectral profiles". J. Quant. Spectrosc. Radiat. Transfer. 1972. 12(9): 1331-1342.

[43] A.O. Vyrodov, J. Heinze, U.E. Meier. "Collisional broadening of spectral lines in the A-X (0-0) system of NO by N2, Ar, and He at elevated pressures measured by laser-induced fluorescence". J. Quant. Spectrosc. Radiat. Transfer. 1995. 53(3): 277-287.

[44] H. Margenau, W.W. Watson. "Pressure effects on Spectral Lines". Rev. Mod. Phys. 1936. 8(1): 22-54.

[45] E. Lindholm. "Pressure broadening of spectral lines" Ark. Mat. Astr. Fys. 1945. 32A(17): 1-18.

[46] P.W. Anderson. "A method of synthesis of the statistical and impact theories of pressure broadening". Phys. Rev. 1952. 86(5): 809.

[47] B.R. Lewis, R. Berzins, C.J. Dedman, T.T. Scholz, J.H. Carver. “Pressure-broadening in the Schumann-Runge bands of molecular oxygen”. J. Quant. Spectrosc. Radiat. Transfer. 1988. 39(4): 271-282.

[48] B. Kleman, E. Lindholm. “The Broadening of Na Lines by Argon”. Ark. Astron. Och. Fys. 1945. 32B (10).

[49] G. Herzberg, “Elementary discussion of electronic states and electronic transition”. In: D. Van Nostrand. Molecular spectra and molecular structure, I Spectra of diatomics molecules, Princeton: D. Van Nostrand Company, INC, 1950., Chap 4, 208

[50] R.J. Kee, J.F. Grcar, M.D. Smooke, J.A. Miller. “A Fortran program for modeling steady laminar one dimensional premixed flames” Sandia Report No. SAND-85-8240. 1985 Sandia National Laboratories.

[51] R.J. Kee, F.M. Rupley, J.A. Miller. “CHEMKIN-II: A Fortran chemical kinetics package for the analysis of gas phase chemical kinetics”. Sandia Report No. SAND-89-8009. 1989. Sandia National Laboratories.

[52] G.P. Smith, D.M. Golden, M. Frenklach, N.W. Moriarty, B. Eiteneer, M. Goldenberg, C.T. Bowman, R.K. Hanson, S. Song, W.C. Gardiner Jr., V.V. Lissianski, Z. Qin http://www.me.berkeley.edu/gri_mech/.

[53] F. Di Teodoro, R.L. Farrow, “CO^+ $B^2\Sigma^+$ (v=0) emission induced by laser excitation of neutral CO at 230 nm”, J. Chem. Phys. 2001. 114(8): 3421-3428.

[54] A.O. Vyrodov, J. Heinze, M. Dillmann, U.E. Meier, W. Stricker. “Laser-induced fluorescence thermometry and concentration measurements on NO A-X(0,0) transitions in the exhaust gas of high pressure CH_4/air flames”. Appl. Phys. B. 1995. 61(5): 409-414.

[55] R. Ciuryło, J. Szudy. “Line-mixing and collision-time asymmetry of spectral line shapes”. Phys. Rev. A. 2001. 63(4): 042714.

TABLES

	$X^1\Sigma^+$	$B^1\Sigma^+$	$C^1\Sigma^+$
T_0	0	86916.198	91919.0639
B_0	1.9225	1.9481153	1.943425
$D_0 \times 10^6$	6.1211	6.7133	6.172
$H_0 \times 10^{12}$	5.7536		
$L_0 \times 10^{17}$	1.0340		

Table 1. Spectroscopic constants (cm^{-1}) for $X^1\Sigma^+$ [8], $B^1\Sigma^+$ and $C^1\Sigma^+$ [9]. B_0 is the rotational constant of v=0, D_0 is the centrifugal distortion constant, H_0 and L_0 are respectively the energy term correction at the 3rd and 4th order.

	$B^1\Sigma$		$A^1\Pi$	
Partner	σ_Q (Å^2)	n	σ_Q (Å^2)	n
N_2	25.10	0.12	44 (a), 59 (b)	
O_2	89.28	-0.06		
CO	36.69	0.02	130 (b)	
H_2O	169.4	-0.44		
CO_2	134.7	-0.33		
CH_4	89.04	-0.16		

Table 2. Cross-section for quenching and temperature exponent (n) of CO $B^1\Sigma^+$ [20] and $A^1\Pi$ state. (a) for v'=0 [21], (b) for v'=9 [22]

	2γ ($cm^{-1}.atm^{-1}$)	m	δ ($cm^{-1}.atm^{-1}$)	n
N_2	0.73	0.77	0.22	0.53
CO	0.74	0.65	0.21	0.52
CO_2	0.77	0.63	0.17	0.75

Table 3. Broadening (2γ), shift (δ) coefficients and temperature exponents (m and n) for CO B(0)-X(0) transition [28].

P(MPa) / T(K)	0.1	0.3	0.5	0.7	1	1.3
300	L	L	L	N.D	N.D	N.D
600	V	L	L	L	N.D	N.D
860	V	L	L	L	N.D	N.D
1750	V	V	V	V	V	V
2000	V	V	V	V	V	V

Table 4. Validity domain of Voigt (V) and Lindholm (L) profile as the function of temperature and pressure. N.D: not defined

FIGURES

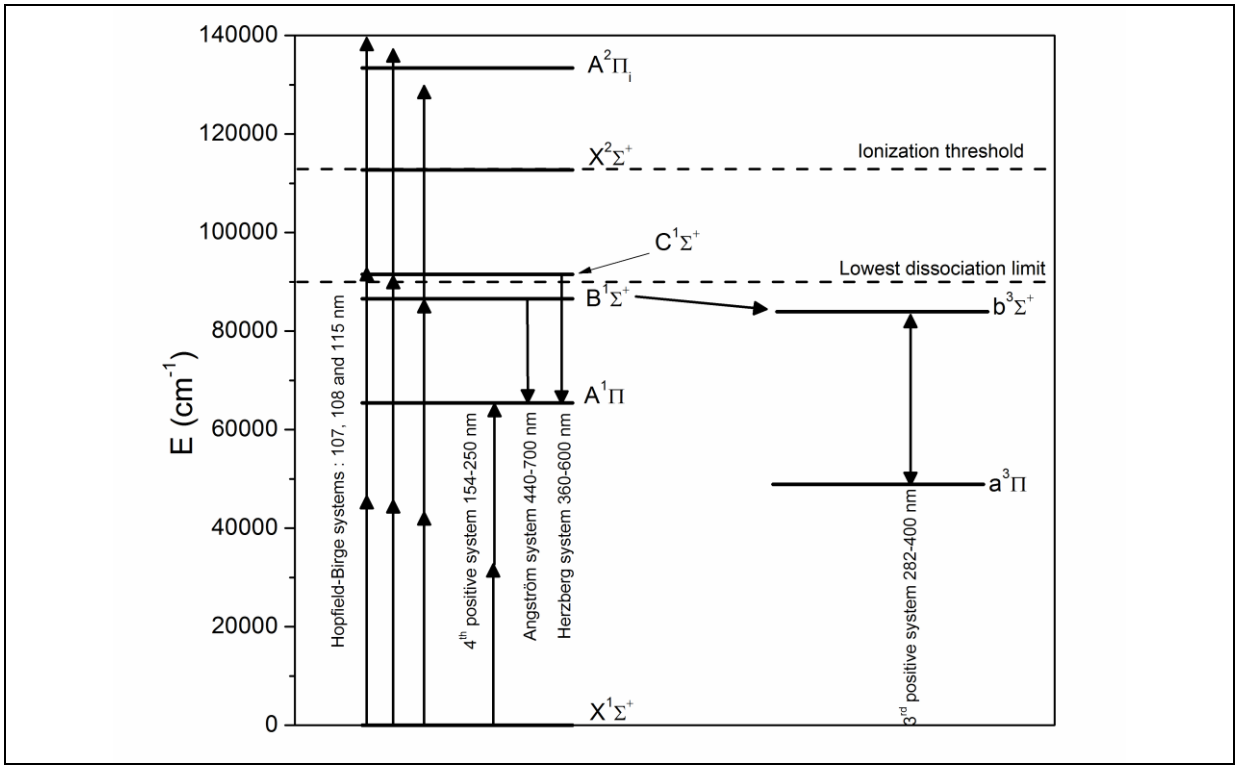

Fig. 1 Simplified energy level diagram of the CO molecule.

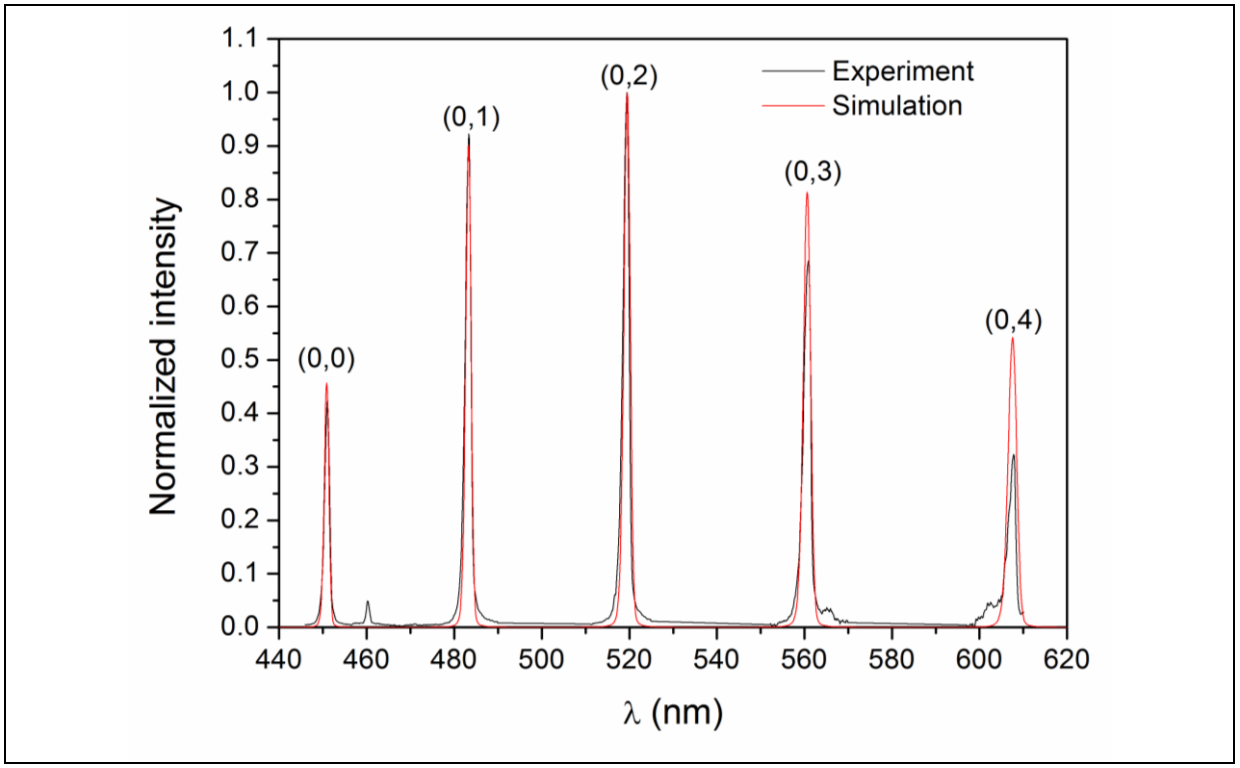

Fig. 2 Comparison between simulated and experimental fluorescence spectra at 300 K and 0.1 MPa.

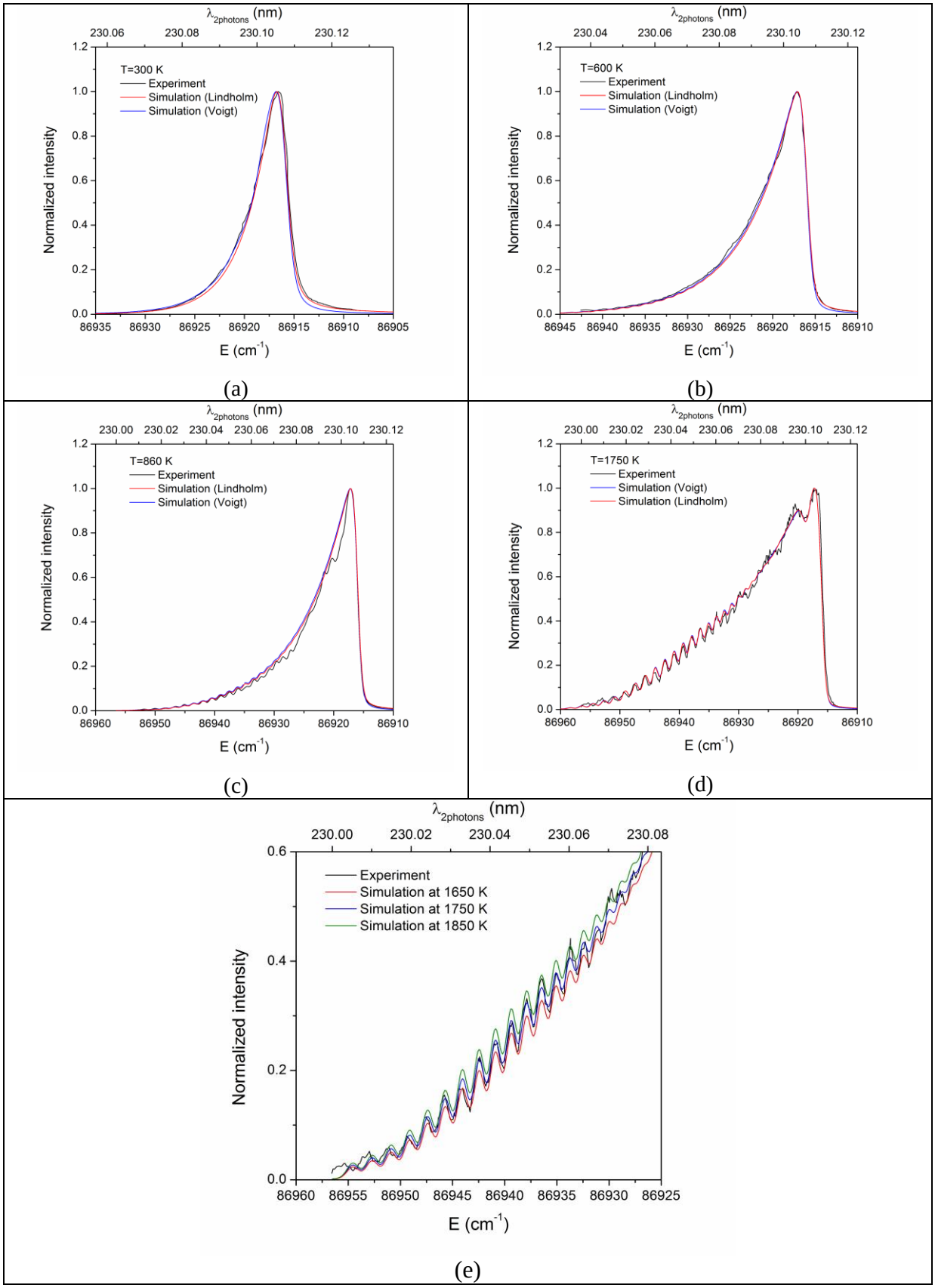

Fig. 3 Comparison between simulated and experimental excitation spectra at 300 K (a), 600 K (b), 860 K (c), 1750 K (d) and 0.1 MPa, Comparison of the rotational structure measured in a CH_4/air flame with simulation at 1650, 1750 and 1850 K at 0.1 MPa (e).

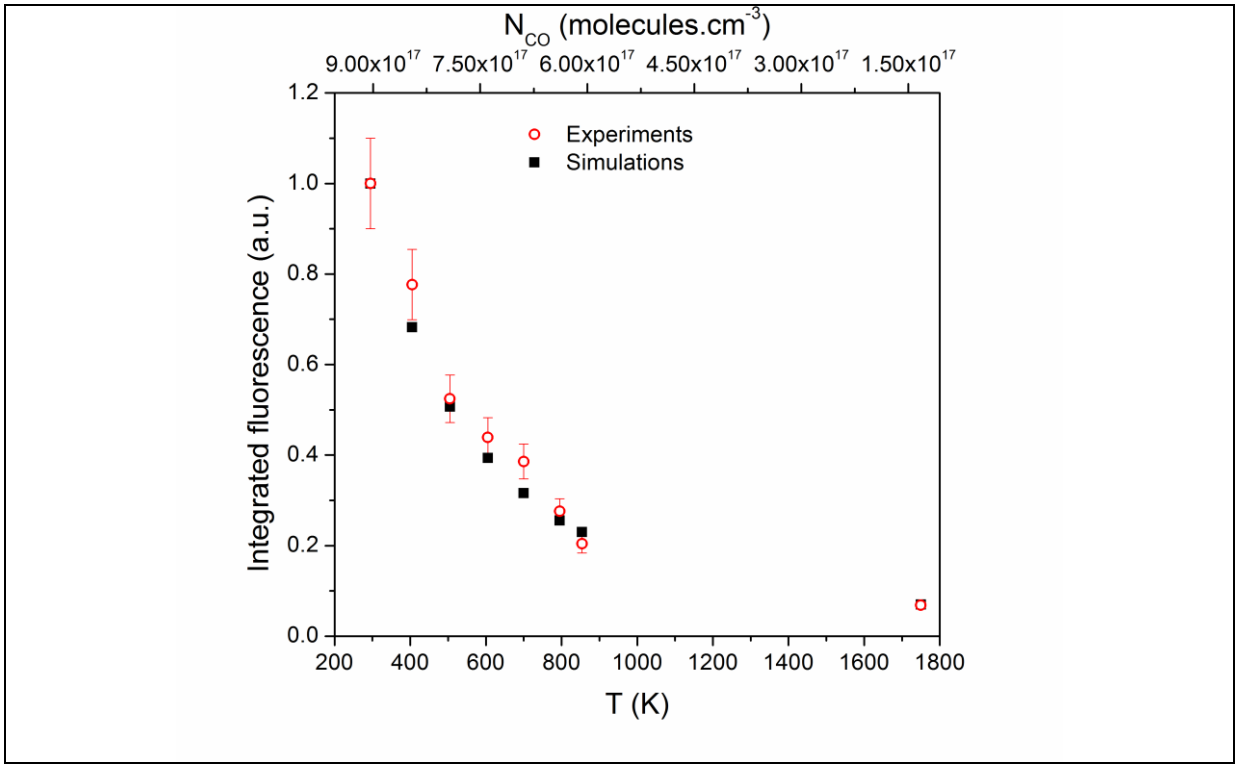

Fig. 4 Evolution of integrated fluorescence with temperature at 0.1 MPa: comparison between simulation and experiments.

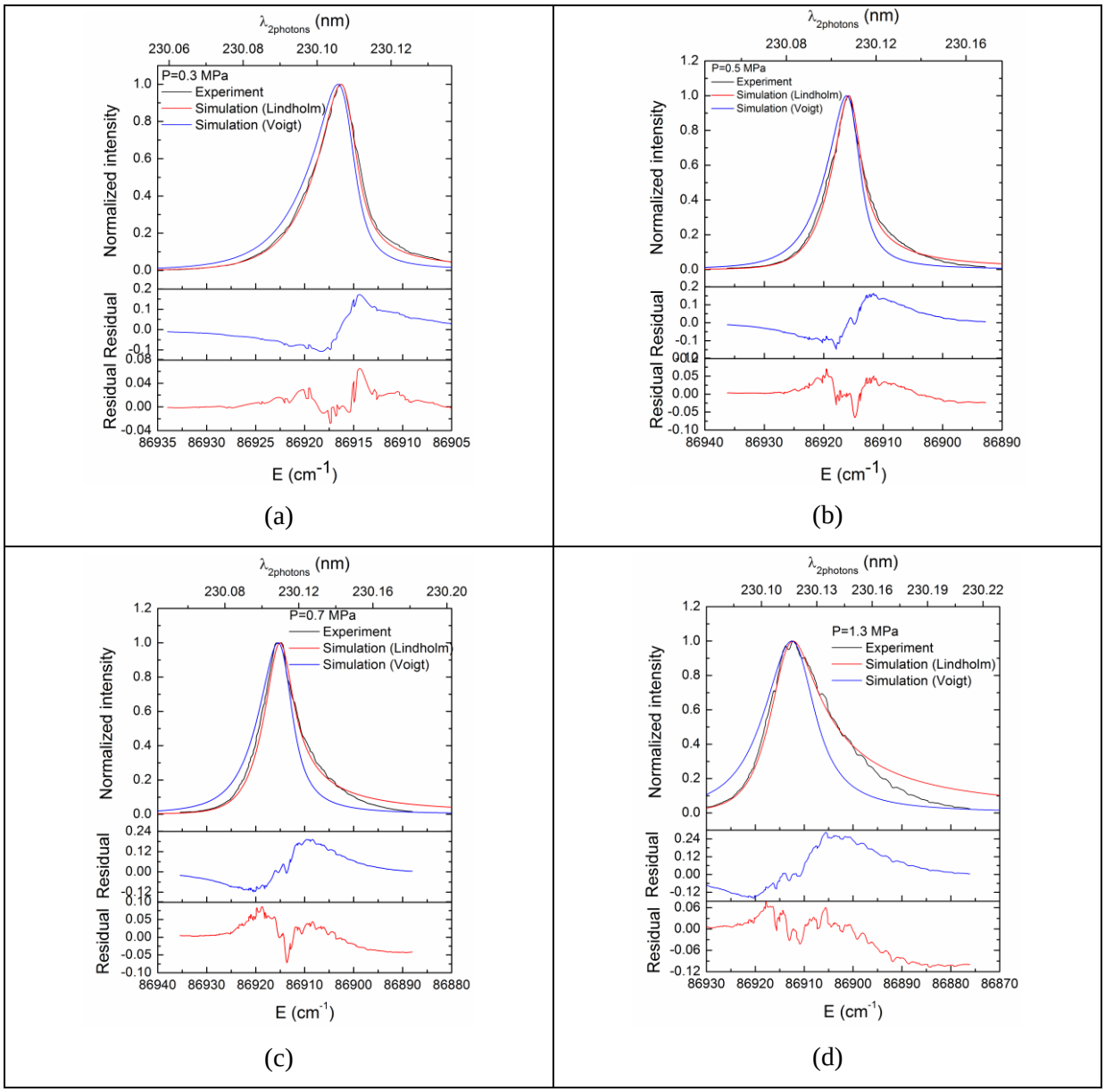

Fig. 5 Comparison between simulated (Voigt and Lindholm profiles) and experimental excitation spectra at 0.3 MPa (a), 0.5 MPa (b), 0.7 MPa (c) and 1.3 MPa (d) and 300 K. Upper residual for Voigt profile and lower residual for Lindholm profile.

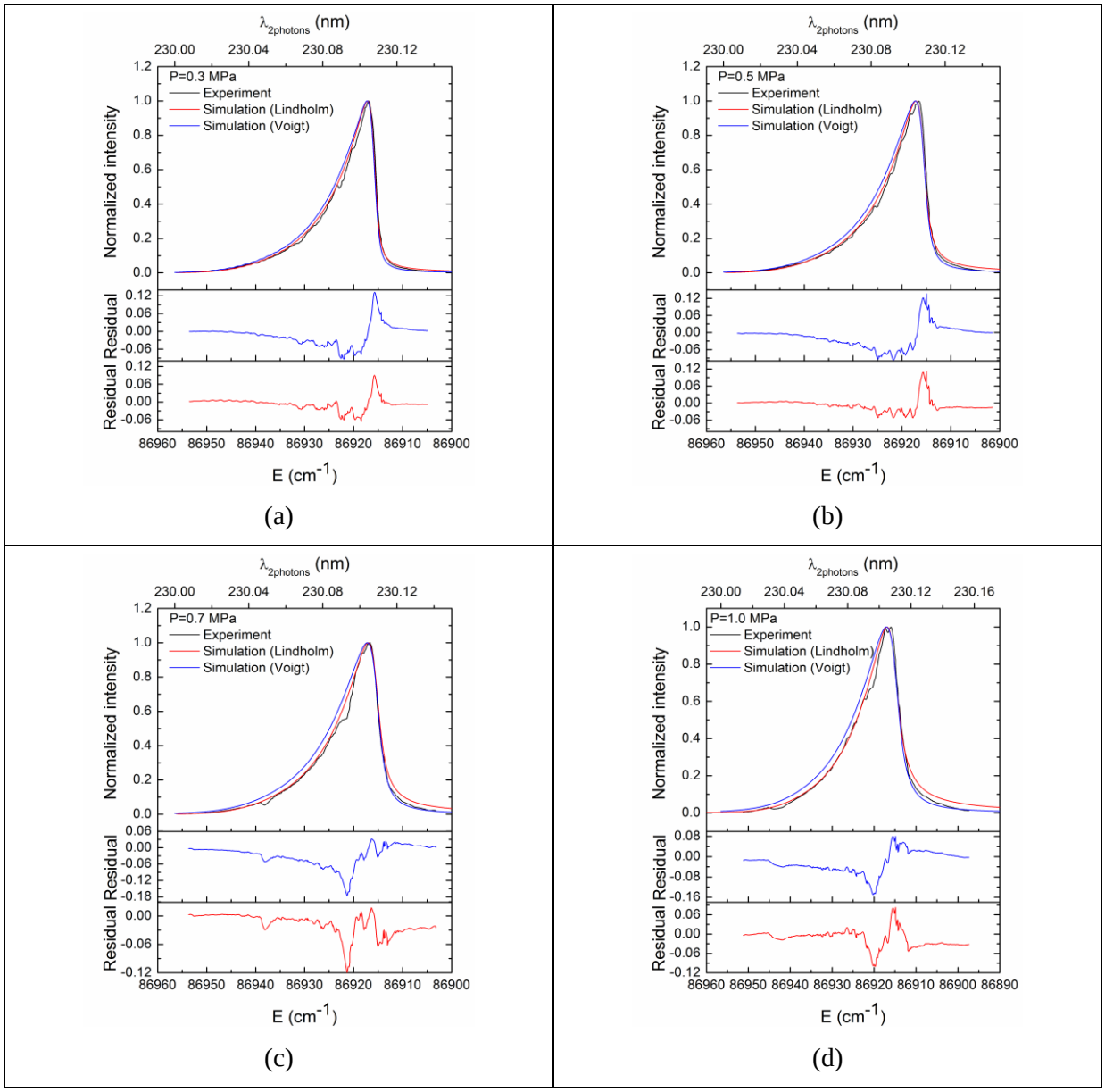

Fig. 6 Comparison between simulated (Voigt and Lindholm profiles) and experimental excitation spectra at 0.3 MPa (a), 0.5 MPa (b), 0.7 MPa (c) and 1 MPa (d) and 860 K. Upper residual for Voigt profile and lower residual for Lindholm profile.

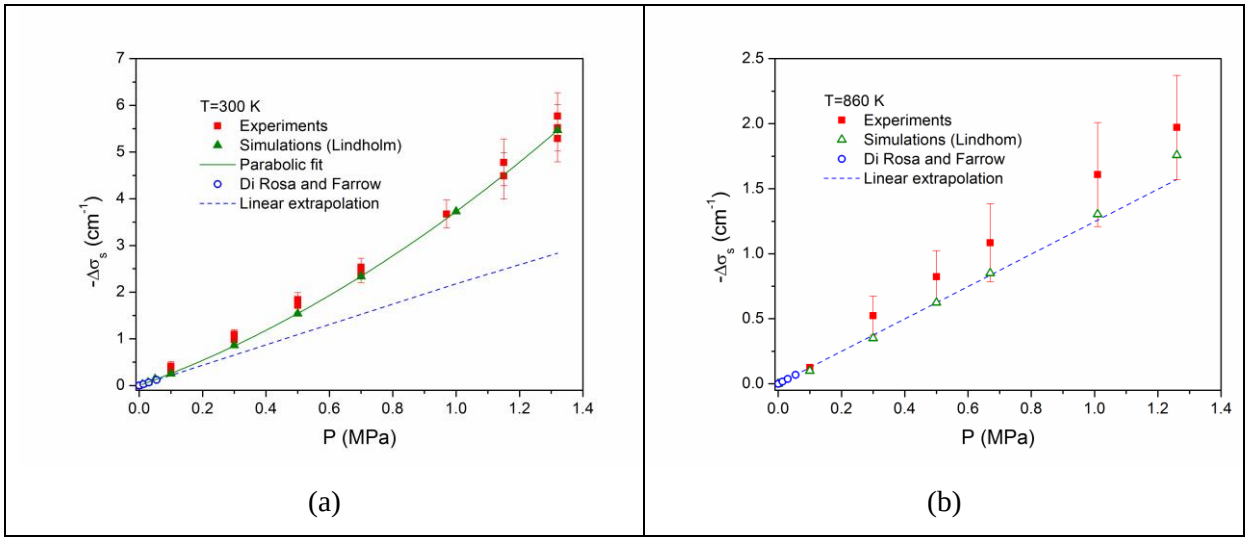

Fig. 7 Evolution of collisional shift with pressure at 300 K (a) and 860 K (b): comparison between simulation and experiments. P=0.1 MPa is taken as reference.

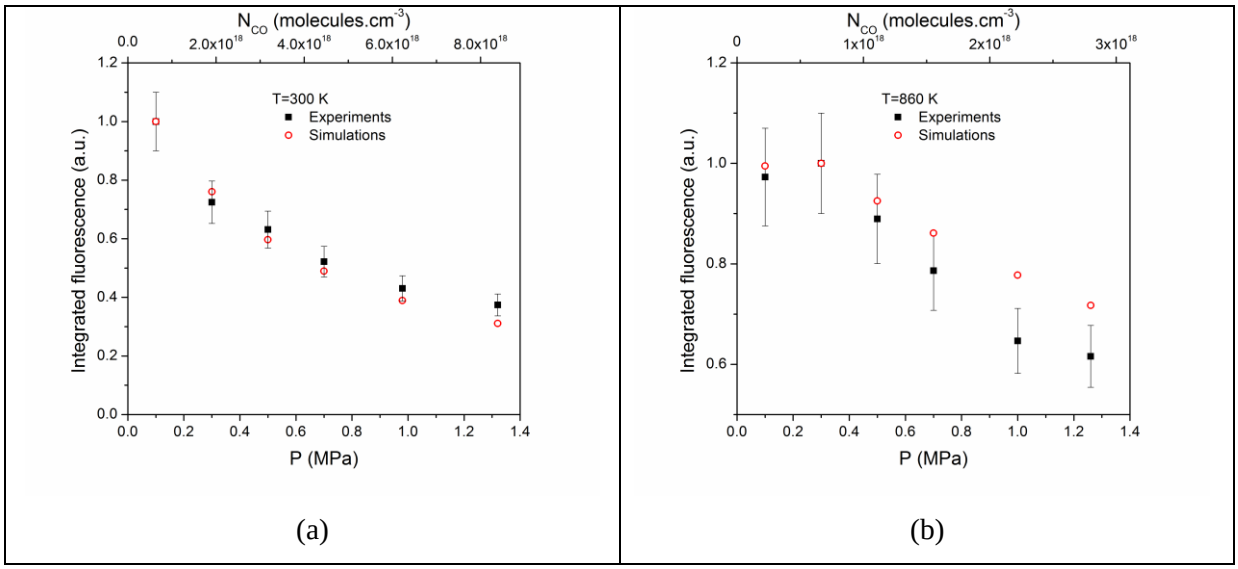

Fig. 8 Evolution of integrated fluorescence with pressure at 300 K (a) and 860 K (b): comparison between simulation and experiments.